Supplemental Material

Testing the Renormalization of the von Klitzing Constant by Cavity Vacuum Fields

Josefine Enkner,[1,2,*] Lorenzo Graziotto,[1,2,*] Felice Appugliese,[1,2] Vasil Rokaj,[3,4] Jie Wang,[5] Michael Ruggenthaler,[6] Christian Reichl,[7] Werner Wegscheider,[7] Angel Rubio,[6,8] and Jérôme Faist[1,2]

[1] *Institute of Quantum Electronics, ETH Zürich, 8093 Zürich, Switzerland*
[2] *Quantum Center, ETH Zürich, 8093 Zürich, Switzerland*
[3] *ITAMP, Center for Astrophysics | Harvard & Smithsonian, MA 02138 Cambridge, USA*
[4] *Department of Physics, Harvard University, MA 02138 Cambridge, USA*
[5] *Department of Physics, Temple University, Philadelphia, Pennsylvania, 19122, USA*
[6] *Max Planck Institute for the Structure and Dynamics of Matter, 22761 Hamburg, Germany*
[7] *Laboratory for Solid State Physics, ETH Zürich, 8093 Zürich, Switzerland*
[8] *Center for Computational Quantum Physics, Flatiron Institute, NY 10010 New York, USA*

I. WHEATSTONE BRIDGE CIRCUITAL RELATION

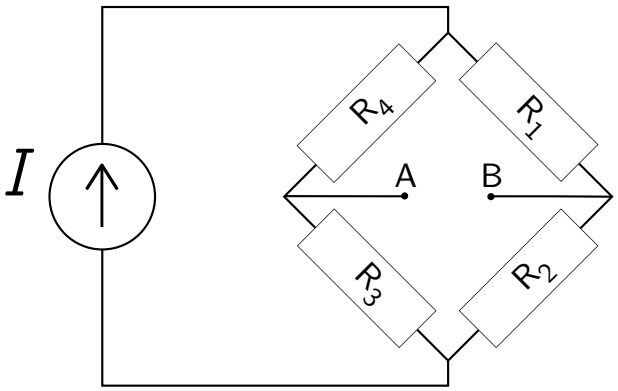

FIG. S1. Circuital scheme of the Wheatstone bridge.

In Figure S1 we display the lumped-element circuit model of the Wheatstone bridge, from which one can obtain the relation given in Eq. 1 in the main text. By Kirchhoff's laws one obtains the unbalance voltage

$$V_{\mathrm{AB}} = \frac{R_1 R_3 - R_4 R_2}{R_1 + R_2 + R_3 + R_4} I, \tag{1}$$

and assuming that all resistors but R_4 are equal, $R_1 = R_2 = R_3 = R_H$, while $R_4 = R_H + \Delta R_H$,

$$\frac{|V_{\mathrm{AB}}|}{I} = \frac{\Delta R_H}{4}. \tag{2}$$

The measurement of the unbalance voltage is meaningful only at the quantum Hall plateaux, where the value of the resistance of the Hall bars not embedded in the cavity is the same and equal to $R_H = h/(e^2\nu)$, with ν being the filling factor. By inverting the previous equation one then obtains

$$\frac{\Delta R_H}{R_H} = 4\frac{|V_{\mathrm{AB}}|}{I}\frac{e^2}{h}\nu, \tag{3}$$

which is Eq. 1 of the main text, where the unbalance voltage $|V_{\mathrm{AB}}|$ is given by the average value $\langle V_{\mathrm{ub}}\rangle$ at the plateau of integer filling factor ν.

II. UNBALANCE VOLTAGE TRACES OF ALL SAMPLES

In Figure S2 we report the measurement of the in-phase quadrature of the unbalance voltage V_{ub} as a function of filling factor (that is of magnetic field, to be read on the top axis) of the reference (S1-S2) and cavity (S3-S5) samples. In order to highlight the values close to zero in the plateaux regions (at integer filling factors) we plot the absolute value of V_{ub} in logarithmic scale. As explained in the main text, the averaging of the unbalance voltage is performed at the integer filling factor plateaux, which are identified by taking the range of magnetic field in which $\log_{10}(|V_{\mathrm{ub}}|/1\,\mathrm{V}) < -8.5$ ($-170\,\mathrm{dB}$), i.e. $|V_{\mathrm{ub}}| < 3.2\,\mathrm{nV}$. This choice is made to ensure that the plateau region is

* J.E. and L.G. contributed equally to this work.

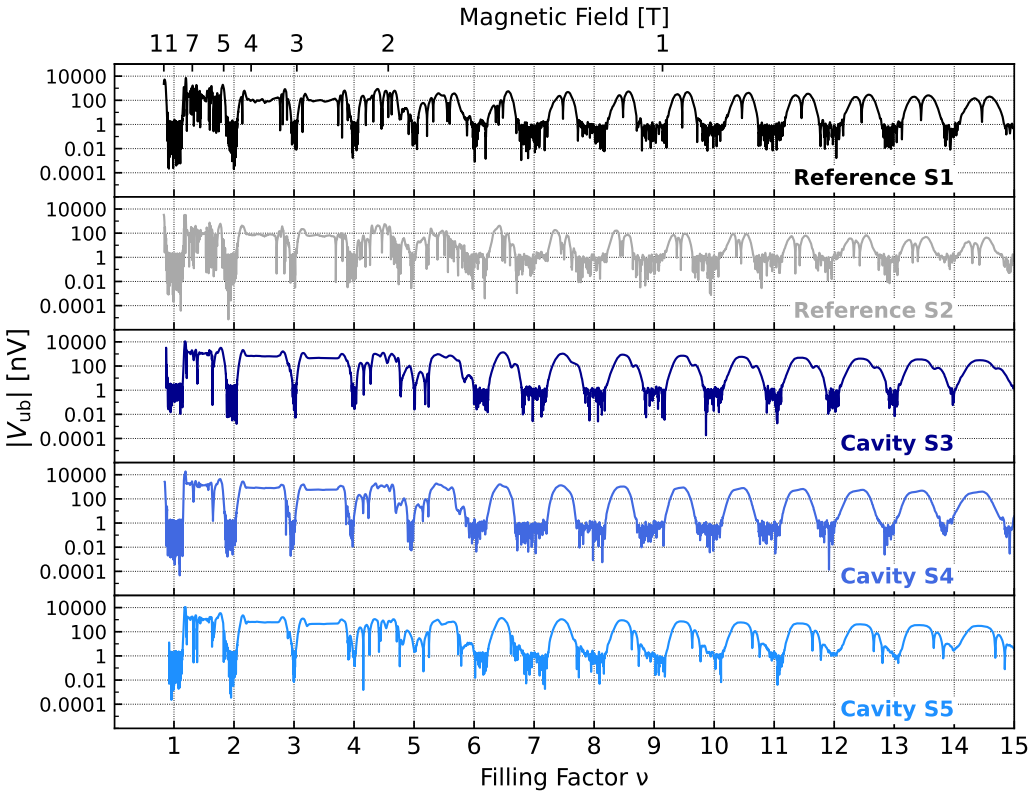

FIG. S2. Absolute value of the unbalance voltage as a function of filling factor for the reference (S1-S2) and cavity (S3-S5) samples. Notice that the voltage axis is in logarithmic scale, to clarify how close is the value to zero at the integer filling factor plateaux.

flat for all the samples, and allows to clearly distinguish its boundaries. Notice that the extension of the plateaux regions decreases with increasing filling factor, so that a plateau cannot be safely identified for filling factors greater than 12. Moreover, we notice some variation in the extension of the plateaux also between different samples, which will reflect in the higher standard deviation of the average, as shown below. As already discussed in the main text, the differences in the values away from the plateaux regions arise due to the electronic density inhomogeneities of the 2DES in which the Hall bars are etched. In Figure S3 we report the averages of the unbalance voltage for the integer filling factor plateaux. The error-bars represent the standard deviation of the mean keeping into account also systematic uncertainties, as discussed in Section III. We notice that for both reference and cavity samples the values oscillate around zero, without showing any behaviour as a function of filling factor. Reference S1 and cavity S4 samples display the narrowest region of oscillation around zero, with a maximum distance of two standard deviations (i.e. they are compatible with zero within a 95% confidence interval), except for filling factor 12 for S4, though cavity sample S3 is zero within one standard deviation at this filling factor. Since no deviation is observed for at least one cavity sample, this already provides an upper bound to the renormalized value of the von Klitzing constant. Reference S2 and cavity S3 and S5 samples show a larger range of oscillation around zero, and S5 in particular is consistently above zero, even if the distance is below three standard deviations (i.e. it is zero within a 99.7% confidence interval). We ascribe this behaviour to the worse performance of the pre-amplifier channel employed to measure S5, which is introducing a larger phase error, thus the out-of-phase component partially leaks into the in-phase component (see Sec. III), giving a finite positive offset. To a lower extent, also S3 displays a similar issue.

III. NATURE OF THE UNCERTAINTIES

There are two main sources of uncertainty which limit the precision and the accuracy of the experiment: one is statistical, and it is given by the fluctuations of the voltage in the plateaux regions due to the voltage noise of the

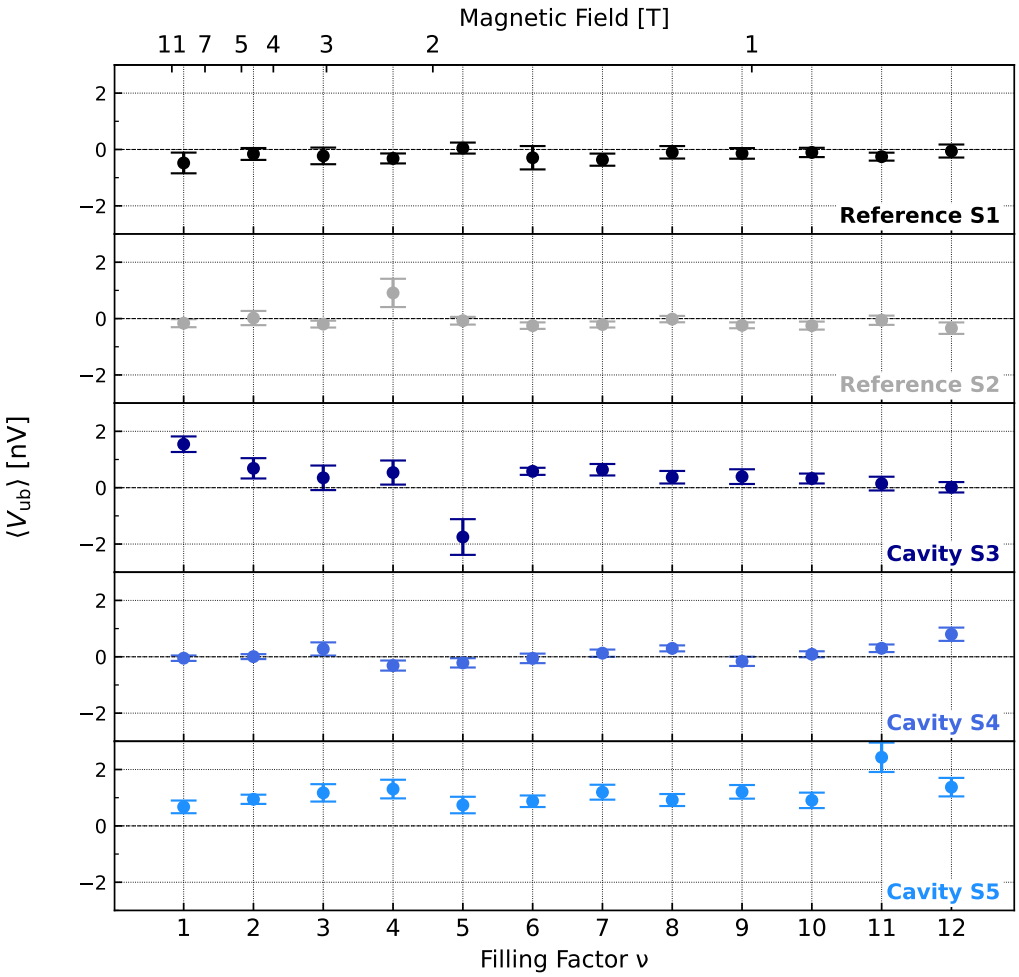

FIG. S3. Average value of the unbalance voltage at the integer filling factor plateaux for the reference (S1-S2) and cavity (S3-S5) samples. The error-bars are given by the standard deviation of the values measured in the plateaux regions, and they have a similar length, given by the 0.7 nV noise level.

AC pre-amplifier, the other one is systematic, and it arises due to inaccuracies of the measurement setup, or to sample-specific characteristics, such as the different contact resistances, or capacitative effects arising in the 2DES. Assuming that the uncertainty sources are independent, we can obtain, for each plateau, the total uncertainty on the unbalance voltage (expressed with the standard deviation, which is represented via error-bars in Fig. S3) as $\sigma_V = \sqrt{\sigma^2_{\text{noise}} + \sigma^2_{\text{offset}} + \sigma^2_{\text{sample}}}$, and we proceed to discuss the meaning of the terms in the following.

The term σ_{noise} is the standard deviation of the average value of the unbalance voltage in the plateau, and it is statistical in nature. If successive data points were uncorrelated it would simply be $\sigma_{\text{noise}} = \sigma^{\text{uncorr}}_{\text{noise}} = \sqrt{\delta V_{\text{ub}}/N}$, where N is the number of data points acquired in the plateau, and δV_{ub} is their sample variance, which is equal to the 0.7 nV pre-amplifier voltage noise (see the Materials and Methods appendix in the main text). However, the data display some correlation due to the fact that the magnetic field is increased at a rate between 10 and 50 mT/min (increasing with increasing field), and the fourth-order low pass filter employed for lock-in demodulation has a settling time equal to about 10 times TC, that is 10 s. Hence we perform a blocking statistical analysis to properly take into account the correlations, and we obtain an uncertainty which is about an order of magnitude greater than $\sigma^{\text{uncorr}}_{\text{noise}}$ and, for filling factors greater or equal to 3, gives the dominant contribution to the total uncertainty.

The term σ_{offset} represents the offset which may be introduced by inaccuracies in the measurement setup. It is systematic in nature, and to assess it we measure the unbalance voltage of a short positioned in place of the sample.

We obtain an estimate of $\sigma_{\text{offset}} = 0.07\,\text{nV}$. The pre-amplifier channel could however also introduce a slight phase error, which combined with a non-zero out-of-phase component of the signal (see below) could give rise to a finite offset in the in-phase component.

Finally, the term σ_{sample} is the systematic uncertainty arising from sample-specific characteristics. As already discussed in the main text, the multiple connection technique [1] allows to reduce the relative inaccuracy introduced by the different contact resistances down to $(R_C/R_H)^4$, where $R_H = h/(e^2\nu)$ is the quantized Hall resistance of the plateau, and R_C is the contact resistance, which varies between 200 and 300 Ω (measured via the three-terminal measurement scheme). Due to capacitative effects of the 2DES the out-of-phase quadrature of the signal V_Y is different from zero in the plateau regions, with values between 2 and 10 nV (increasing with decreasing filling factor). Being it out-of-phase it should not bear any impact on the in-phase quadrature of the unbalance voltage V_X (displayed in Fig. S2), however being the in-phase component much lower than the out-of-phase one, the latter can partially contribute to a non-zero value of the former due to the slight phase shift introduced by the pre-amplifier channels. We assess this uncertainty from the reference samples, where we estimate a deviation of the out-of-phase component from the 90 degrees phase up to 10 degrees, so that the in-phase component V_X can acquire an offset of $\sqrt{V_X^2 + V_Y^2}\sin(10°)$, which we adopt as σ_{sample}. This uncertainty contribution dominates at the plateaux at filling factors 1 and 2, and we interpret it as an higher reactance of the contacts to the 2DES at higher magnetic fields. The choice of measuring more than one reference/cavity sample (on the same chip) is thus suitable to assess the sample-specific uncertainties, and to statistically treat them. We display in Figure S4 the weighted mean of both reference and cavity samples, along with their standard deviation (the error-bars are three standard deviation-long, so to display the 99.7% confidence interval). The weighted mean $\overline{\langle V_{\text{ub}}\rangle}$ and the standard deviation of the weighted mean $\sigma_{\bar{V}}$ are defined as

$$\overline{\langle V_{\text{ub}}\rangle} = \frac{\sum_i \frac{\langle V_{\text{ub}}\rangle_i}{(\sigma_V)_i^2}}{\sum_i \frac{1}{(\sigma_V)_i^2}}, \qquad \sigma_{\bar{V}} = \sqrt{\frac{1}{\sum_i \frac{1}{(\sigma_V)_i^2}}}, \tag{4}$$

where the sums are extended over all the reference/cavity samples. We can infer that no deviation is observed within a range of 0.7 nV for filling factor 1, which translates to a precision of 1 part in 10^5 for the Hall resistance deviation, as discussed in the main text.

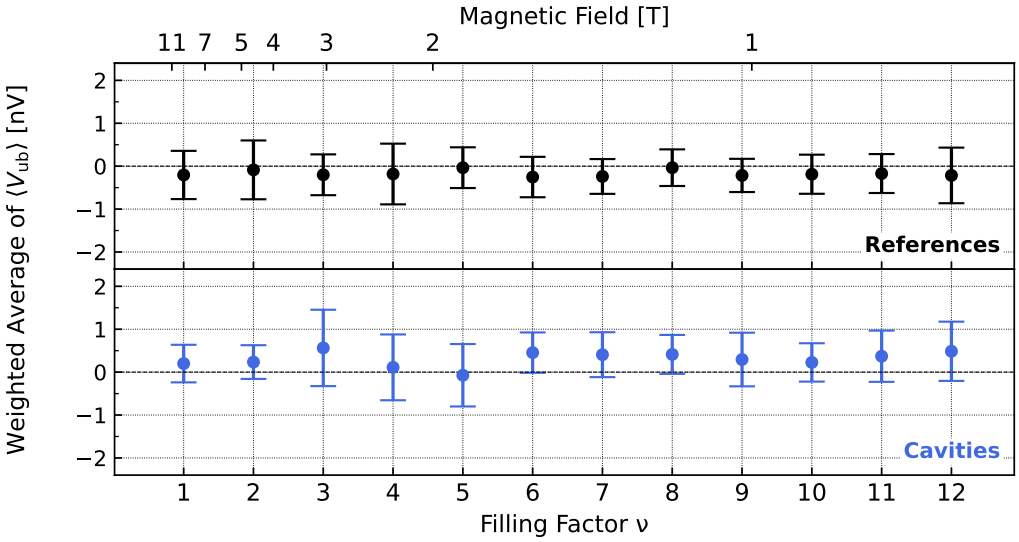

FIG. S4. Weighted averages of the unbalance voltage for reference S1-S2 samples (top panel) and cavity S3-S5 samples (bottom panel), as a function of filling factor. The error-bars are given here by three times the (weighted) standard deviation, i.e. they refer to a 99.7% confidence interval.

IV. TEMPERATURE STUDY

To connect and compare the results of the present work with the ones reported in Ref. [2] we have performed measurements of the unbalance voltage as a function of temperature, in order to extract the activation energy of the Hall resistance deviation from the quantum Hall plateaux [3, 4]. In Ref. [2] we had indeed extracted the activation energy by measuring instead the minima of the longitudinal resistivity as a function of temperature. In Figure S5 we show the unbalance voltage as a function of magnetic field and temperature for the plateaux at filling factor 5-7, for reference S1-S2 and cavity S4-S5 samples (we exclude cavity S3 sample since, as already discussed in Sec. III, its measurement is affected by a larger phase error). Observing the behaviour of the reference samples one can notice how the increase in temperature reduces the length of the plateaux, but does not cause a consistent deviation from quantization. Indeed, as already shown in Ref. [2] for a similar reference sample, which we remind it to be a small 40 µm-wide and 160 µm-long Hall bar, the activation energy at these magnetic fields is of the order of 6 K (therein we had also measured at higher temperatures). On the other hand, cavity samples do display an activated behaviour, with minima of the unbalance voltage lifting with increasing temperature, as shown in Fig. S6 (left). From the exponential fitting of the Arrhenius plot we extract an activation energy (Fig. S6 right) which increases linearly with magnetic field, and which is far lower than the reference one, and lower also than the one of cavity samples having a lower normalized coupling.

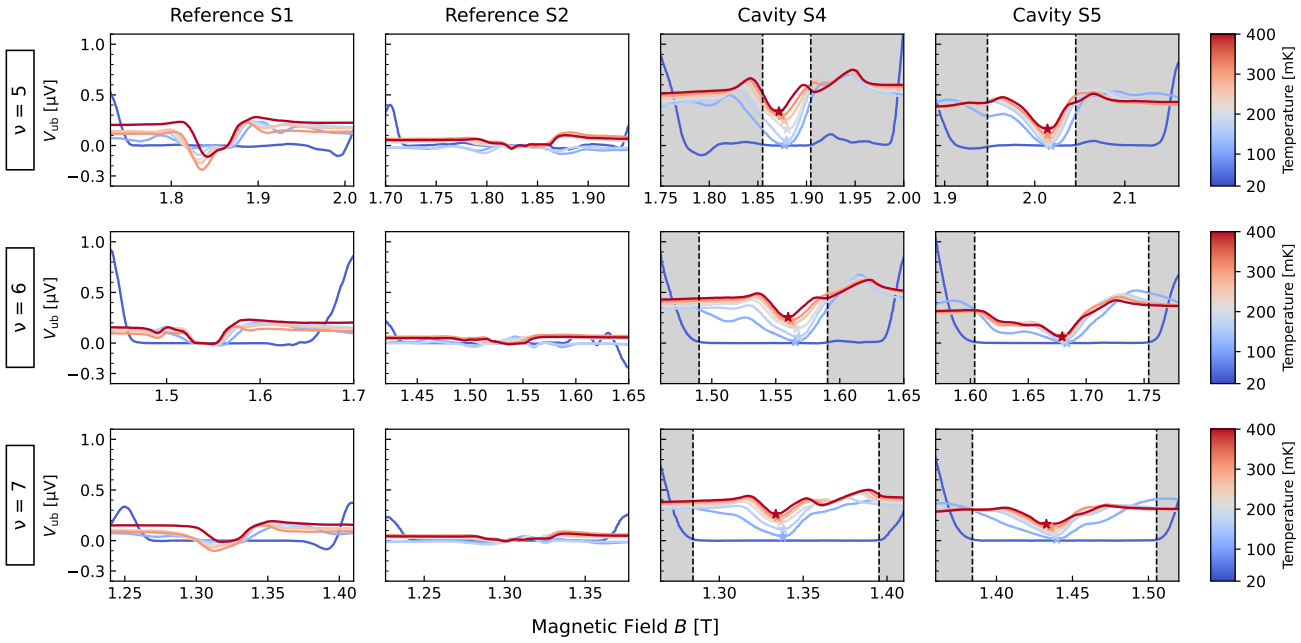

FIG. S5. Unbalance voltage for reference S1-S2 and cavity S4-S5 samples (varied along rows), as a function of magnetic field and of temperature (displayed using color following the color-bars to the right), for filling factors $\nu = 5 - 7$ (varied along columns). Observe how reference samples do not consistently display a loss of plateau quantization by increasing the temperature – though increasing the temperature causes a reduction in the plateaux length – as opposed to cavity samples, where the minimum of the unbalance voltage in the plateaux regions (white area in between the two vertical dashed lines) increases when increasing the temperature. The minima are marked with a star, and are then displayed as a function of inverse temperature in Fig. S6.

V. THEORETICAL BACKGROUND

A. Homogeneous 2D Quantum Hall System Coupled to the Cavity

We consider a homogeneous, two-dimensional electron gas coupled to a strong magnetic field and a single-mode homogeneous cavity field. The system is described by the Pauli-Fierz Hamiltonian [5, 6]

$$\hat{H} = \sum_{i=1}^{N} \frac{\left(\boldsymbol{\pi}_i + e\hat{\mathbf{A}}\right)^2}{2m} + \hbar\omega_{\mathrm{cav}} \left(\hat{a}^\dagger \hat{a} + \frac{1}{2}\right) + \sum_{i<j} W(\mathbf{r}_i - \mathbf{r}_j), \tag{5}$$

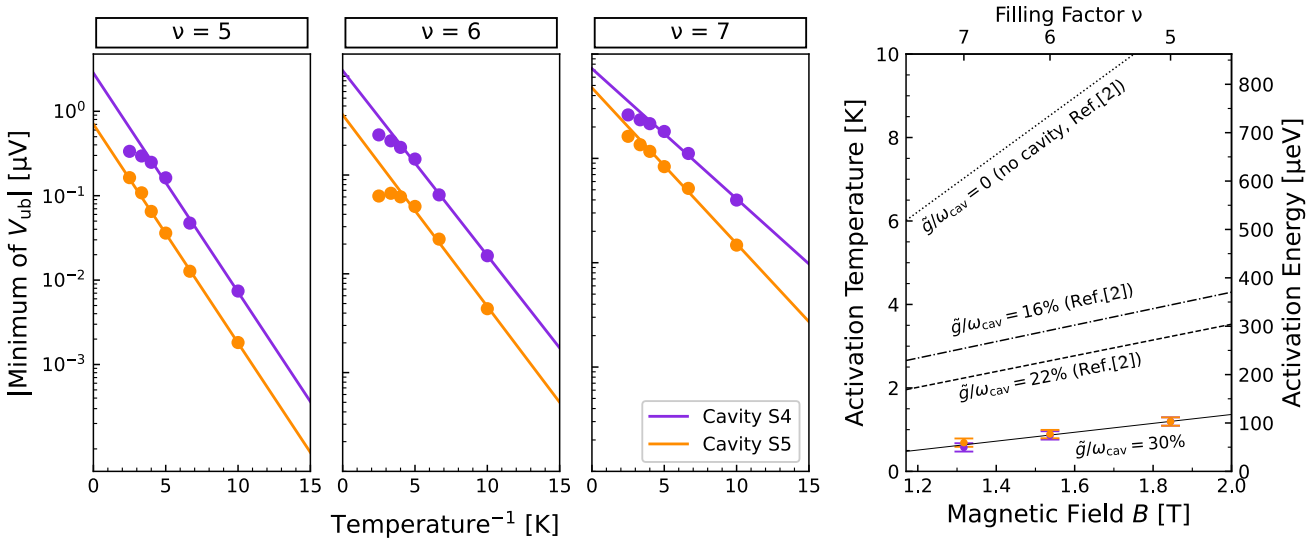

FIG. S6. Left: Arrhenius plots for cavity S4-S5 samples, i.e. absolute value of the minimum of the unbalance voltage (displayed in log scale) as a function of inverse temperature. The minima are taken from the points marked with a star in Fig. S5. Right: Activation energy as a function of magnetic field for cavity S4-S5 samples as extracted from the exponential fit of the absolute value of the minima of the unbalance voltage. The black solid line indicates a linear fit of the activation energy as a function of magnetic field for cavity S4-S5 samples studied in the present work, which display a normalized coupling $\tilde{g}/\omega_{\rm cav} \simeq 30\%$. In the same plot we report the linear fits of the activation energy measured for a reference sample (zero coupling, dotted line), a cavity sample with 16% normalized coupling (dashed-dotted line), and a cavity sample with 22% normalized coupling (dashed line), as obtained in Ref. [2] (see supplemental material therein), employing a different measurement technique (as discussed in the main text). Notice how the cavity activation energy is far below the reference one, and that the higher the coupling the lower the activation energy.

where $\boldsymbol{\pi}_i = \mathrm{i}\hbar\boldsymbol{\nabla}_i + e\mathbf{A}_{\rm ext}(\mathbf{r}_i)$ are the dynamical momenta of the electrons and $\mathbf{A}_{\rm ext}(\mathbf{r}) = -\mathbf{e}_x By$ describes the homogeneous magnetic field $\mathbf{B} = \boldsymbol{\nabla} \times \mathbf{A}_{\rm ext}(\mathbf{r}) = B\mathbf{e}_z$. The cavity field $\hat{\mathbf{A}} = \sqrt{\frac{\hbar}{2\epsilon_0 \mathcal{V}\omega_{\rm cav}}}\mathbf{e}_x \left(\hat{a} + \hat{a}^\dagger\right)$ is characterized by the in-plane polarization vector $\mathbf{e}_x$ and the cavity frequency $\omega_{\rm cav}$. The $\mathcal{V}$ and ϵ_0 are the effective mode volume and the dielectric constant, respectively, and the ladder operators $\hat{a}$ and $\hat{a}^\dagger$ represent the bare photon fields. With Galilean invariance in a purely homogeneous system, the center of mass (CM) is decoupled from the relative motion of the electrons, regardless of the interaction strength [7]. To demonstrate this we use the CM and relative distance coordinates

$$\mathbf{R} = \frac{1}{\sqrt{N}}\sum_{i=1}^{N}\mathbf{r}_i \;\text{ and }\; \widetilde{\mathbf{r}}_j = \frac{\mathbf{r}_1 - \mathbf{r}_j}{\sqrt{N}} \;\text{ with }\; j > 1. \tag{6}$$

The Hamiltonian in the new frame is the sum of two parts: (i) the CM part $\hat{H}_{\rm cm}$ which is coupled to the quantized field $\hat{\mathbf{A}}$ and (ii) the relative distances $\hat{H}_{\rm rel}$ which does not couple to the cavity field, $\hat{H} = \hat{H}_{\rm cm} + \hat{H}_{\rm rel}$ where each part looks as

$$\hat{H}_{\rm cm} = \frac{1}{2m}\left(\mathrm{i}\hbar\nabla_{\mathbf{R}} + e\mathbf{A}_{\rm ext}(\mathbf{R}) + e\sqrt{N}\hat{\mathbf{A}}\right)^2 + \hbar\omega_{\rm cav}\left(\hat{a}^\dagger\hat{a} + \frac{1}{2}\right) \tag{7}$$

$$\hat{H}_{\rm rel} = \frac{1}{2m}\sum_{j=2}^{N}\left(\frac{\mathrm{i}\hbar}{\sqrt{N}}\widetilde{\nabla}_j + e\sqrt{N}\mathbf{A}_{\rm ext}(\widetilde{\mathbf{r}}_j)\right)^2 - \frac{\hbar^2}{2mN}\sum_{j,l=2}^{N}\widetilde{\nabla}_j\cdot\widetilde{\nabla}_l - \frac{e^2}{2m}\left(\sum_{j=2}^{N}\mathbf{A}_{\rm ext}(\widetilde{\mathbf{r}}_j)\right)^2 + \sum_{i<j}W(\mathbf{r}_i - \mathbf{r}_j). \tag{8}$$

From the result above it becomes evident that in the homogeneous limit the quantum cavity field only couples to the CM of the electron gas while the correlations decouple from it. This implies that all the cavity-matter phenomena happen at the CM.

B. Collective Landau Polaritons

The Hamiltonian $\hat{H}_{\rm cm}$ has the form of two coupled harmonic oscillators, one for the Landau level transition and one for the photons. In many cases such a Hamiltonian is known as the Hopfield Hamiltonian which can be solved by the Hopfield transformation [8]. After the Hopfield transformation we find

$$\hat{H}_{\rm cm} = \hbar\Omega_+ \left(\hat{b}_+^\dagger \hat{b}_+ + \frac{1}{2}\right) + \hbar\Omega_- \left(\hat{b}_-^\dagger \hat{b}_- + \frac{1}{2}\right) \tag{9}$$

where $\{\hat{b}_\pm^\dagger, \hat{b}_\pm\}$ are the creation and annihilation operators of the Landau polariton quasiparticles. The $\Omega_\pm$ are the upper and lower Landau polariton modes respectively,

$$\Omega_\pm^2 = \frac{\omega_{\rm cav}^2 + \omega_d^2 + \omega_{\rm cyc}^2}{2} \pm \sqrt{\omega_d^2\omega_{\rm cyc}^2 + \left(\frac{\omega_{\rm cav}^2 + \omega_d^2 - \omega_{\rm cyc}^2}{2}\right)^2} \tag{10}$$

where $\omega_d = \sqrt{e^2 N/m_e\epsilon_0\mathcal{V}}$ is the diamagnetic frequency originating from the $\hat{\mathbf{A}}^2$ which depends on the number of electrons N and the effective mode volume $\mathcal{V}$. To define the polariton operators we represent the photon annihilation operator in terms of a displacement coordinate q and its conjugate momentum as $\hat{a} = (q + \partial_q)/\sqrt{2}$, with $\hat{a}^\dagger$ obtained via conjugation. In this representation the polariton operators $\{\hat{b}_\pm, \hat{b}_\pm^\dagger\}$ can be written in terms of mixed, polaritonic coordinates as $S_\pm = \sqrt{\hbar/2\Omega_\pm}\left(\hat{b}_\pm + \hat{b}_\pm^\dagger\right)$ with

$$S_+ = \frac{\sqrt{m_e}\bar{Y} + q\Lambda\sqrt{\hbar/\omega_{\rm cav}}}{\sqrt{1+\Lambda^2}} \text{ and } S_- = \frac{-q\sqrt{\hbar/\omega_{\rm cav}} + \sqrt{m_e}\Lambda\bar{Y}}{\sqrt{1+\Lambda^2}}$$

where $\bar{Y} = Y + \frac{\hbar K_x}{eB}$ is the guiding center and K_x is the electronic wave number in the x-direction. Also we introduced the parameter $\Lambda = \alpha - \sqrt{1+\alpha^2}$ with $\alpha = \left(\omega_{\rm cyc}^2 - \omega_{\rm cav}^2 - \omega_d^2\right)/2\omega_d\omega_{\rm cyc}$ which quantifies the mixing between electronic and photonic degrees of freedom. It is worth noticing that in the limit $\omega_{\rm cav} \to 0$ the lower polariton frequency goes to zero, $\Omega_- \to 0$, which means that the system becomes gapless. In this limit the canonical transformation from the electron and photon basis to the polariton basis becomes singular as it was explained also in Ref. [9].

C. Finite Temperature Kubo Transport

Here we present the Kubo linear-response formalism for the finite temperature transport of the light-matter system. As we already showed the Hamiltonian of our system can be written as a sum of a CM and relative part $\hat{H} = \hat{H}_{\rm cm} + \hat{H}_{\rm rel}$. To proceed we assume that the eigenstates of $\hat{H}_{\rm cm}$ are $|\Phi_n\rangle$ and the eigenstates of $\hat{H}_{\rm rel}$ are $|F_I\rangle$ such that it holds

$$\hat{H}_{\rm cm}|\Phi_n\rangle = E_n|\Phi_n\rangle \text{ and } \hat{H}_{\rm rel}|F_I\rangle = E_I|F_I\rangle \tag{11}$$

Then, the eigenstates of the full Hamiltonian $\hat{H}$ are $|\Psi_{nI}\rangle = |\Phi_n\rangle \otimes |F_I\rangle$, and the full eigenspectrum is $E_{nI} = E_n + E_I$. The Kubo formula for the optical conductivity of the system is [10, 11]

$$\sigma_{ab}(w) = \frac{\mathrm{i}}{w + \mathrm{i}\delta}\left(\frac{e^2 n_e}{m_e}\delta_{ab} + \frac{\chi_{ab}(w)}{A}\right) \quad \delta \to 0^+ \tag{12}$$

where $a, b = x, y, z$. The first term in the optical conductivity is the Drude term, while the second term is the current-current correlator in the frequency domain, which is defined as the Fourier transform of current-current correlator in the time domain

$$\chi_{ab}(t) = \frac{-\mathrm{i}\Theta(t)}{\hbar}\langle[\hat{J}_a(t), \hat{J}_b]\rangle. \tag{13}$$

The current operators are considered in the interaction picture $\hat{\mathbf{J}}(t) = e^{\mathrm{i}Ht/\hbar}\hat{\mathbf{J}}e^{-\mathrm{i}\hat{H}t/\hbar}$ [10]. In the canonical ensemble the expectation value of an operator $\hat{\mathcal{O}}$ is defined as [11]

$$\langle\hat{\mathcal{O}}\rangle = Tr\{\hat{\rho}\hat{\mathcal{O}}\} = \frac{1}{\mathcal{Z}}\sum_{n,I}\langle\Psi_{nI}|e^{-\beta\hat{H}}\hat{\mathcal{O}}|\Psi_{nI}\rangle \tag{14}$$

where the partition function is $\mathcal{Z} = \sum_{n,I} e^{-\beta E_n} e^{-\beta E_I}$. We will use these formulas now for the computation of the current correlation functions. The current response can be splitted into two parts

$$\chi_{ab}(t) = \frac{-\mathrm{i}\Theta(t)}{\hbar}\left(\langle \hat{J}_a(t)\hat{J}_b\rangle - \langle \hat{J}_b\hat{J}_a(t)\rangle\right). \tag{15}$$

Let us compute first the first term $\langle \hat{J}_a(t)\hat{J}_b\rangle$. We use the expression for the canonical ensemble and for the current operator in the interaction picture and we have

$$\langle \hat{J}_a(t)\hat{J}_b\rangle = \frac{1}{\mathcal{Z}}\sum_{n,I} e^{-\beta E_{nI}}\langle \Psi_{nI}|e^{\mathrm{i}Ht/\hbar}\hat{J}_a e^{-\mathrm{i}\hat{H}t/\hbar}\hat{J}_b|\Psi_{nI}\rangle = \frac{1}{\mathcal{Z}}\sum_{n,I} e^{-\beta E_{nI}}e^{\mathrm{i}tE_{nI}/\hbar}\langle \Psi_{nI}|\hat{J}_a e^{-\mathrm{i}\hat{H}t/\hbar}\hat{J}_b|\Psi_{nI}\rangle. \tag{16}$$

We introduce the identity $\mathbb{I} = \sum_{m,J}|\Psi_{mJ}\rangle\langle\Psi_{mJ}|$ in the above expression

$$\begin{aligned}\langle \hat{J}_a(t)\hat{J}_b\rangle &= \frac{1}{\mathcal{Z}}\sum_{n,m,J,I} e^{-\beta E_{nI}}e^{\mathrm{i}tE_{nI}/\hbar}\langle \Psi_{nI}|\hat{J}_a e^{-\mathrm{i}\hat{H}t/\hbar}|\Psi_{mJ}\rangle\langle\Psi_{mJ}|\hat{J}_b|\Psi_{nI}\rangle \\ &= \frac{1}{\mathcal{Z}}\sum_{n,m,J,I} e^{-\beta E_{nI}}e^{\mathrm{i}t(E_{nI}-E_{mJ})/\hbar}\langle \Psi_{nI}|\hat{J}_a|\Psi_{mJ}\rangle\langle\Psi_{mJ}|\hat{J}_b|\Psi_{nI}\rangle \end{aligned}\tag{17}$$

Since we work in the CM frame in order to proceed we need examine how the current operator looks in the CM frame. The full gauge-invariant current operator in the original frame is [12]

$$\hat{\mathbf{J}} = -\frac{\mathrm{i}e\hbar}{m_\mathrm{e}}\sum_{j=1}^{N}\nabla_j - \frac{e^2N}{m_\mathrm{e}}\hat{\mathbf{A}} - \frac{e^2}{m_\mathrm{e}}\sum_{i=1}^{N}\mathbf{A}_\mathrm{ext}(\mathbf{r}_i). \tag{18}$$

Then, the current operator in the CM frame takes the form

$$\hat{\mathbf{J}} = \sqrt{N}\left[-\frac{\mathrm{i}e\hbar}{m_e}\nabla_{\mathbf{R}} - \frac{e^2}{m_e}\sqrt{N}\hat{\mathbf{A}} - \frac{e^2}{m_e}\mathbf{A}_\mathrm{ext}(\mathbf{R})\right] \equiv \hat{\mathbf{J}}_\mathrm{cm}. \tag{19}$$

The above result shows that the total current in the system is equal to current of the CM and depends only on CM related operators. This property has the following important implication

$$\langle \Psi_{nI}|\hat{\mathbf{J}}|\Psi_{mJ}\rangle = \delta_{IJ}\langle\Phi_n|\hat{\mathbf{J}}|\Phi_m\rangle \tag{20}$$

using the above the expression for the current correlator simplifies

$$\langle \hat{J}_a(t)\hat{J}_b\rangle = \frac{1}{\mathcal{Z}}\sum_{n,m,I} e^{-\beta E_{nI}}e^{\mathrm{i}t(E_n-E_m)/\hbar}\langle\Phi_n|\hat{J}_a|\Phi_m\rangle\langle\Phi_m|\hat{J}_b|\Phi_n\rangle \tag{21}$$

To obtain the above we used that $E_{nI} - E_{mI} = E_n - E_m$. To complete the computation we need to multiply $\langle \hat{J}_a(t)\hat{J}_b\rangle$ with $\frac{-\mathrm{i}\Theta(t)}{\hbar}$ and Fourier transform into the frequency space

$$\begin{aligned}\frac{-\mathrm{i}\Theta(t)}{\hbar}\langle \hat{J}_a(t)\hat{J}_b\rangle \longrightarrow \frac{1}{\mathcal{Z}}\sum_{n,m,I} e^{-\beta E_{nI}}\frac{\langle\Phi_n|\hat{J}_a|\Phi_m\rangle\langle\Phi_m|\hat{J}_b|\Phi_n\rangle}{w+(E_n-E_m)/\hbar+\mathrm{i}\delta} &= \frac{\sum_I e^{-\beta E_I}}{\sum_I e^{-\beta E_I}\sum_k e^{-\beta E_k}}\sum_{n,m,I} e^{-\beta E_n}\frac{\langle\Phi_n|\hat{J}_a|\Phi_m\rangle\langle\Phi_m|\hat{J}_b|\Phi_n\rangle}{w+(E_n-E_m)/\hbar+\mathrm{i}\delta} \\ &= \frac{1}{\sum_k e^{-\beta E_k}}\sum_{n,m} e^{-\beta E_n}\frac{\langle\Phi_n|\hat{J}_a|\Phi_m\rangle\langle\Phi_m|\hat{J}_b|\Phi_n\rangle}{w+(E_n-E_m)/\hbar+\mathrm{i}\delta} \ \text{ with } \ \delta\to 0^+. \end{aligned}\tag{22}$$

Following exactly the same procedure for the second term in Eq. 15 $\frac{\mathrm{i}\Theta(t)}{\hbar}\langle \hat{J}_b\hat{J}_a(t)\rangle$ we find the the expression for the current-current response function

$$\chi_{ab}(w) = \frac{1}{\sum_l e^{-\beta E_l}}\sum_{n,m}\left(e^{-\beta E_n} - e^{-\beta E_m}\right)\frac{\langle\Phi_n|\hat{J}_a|\Phi_m\rangle\langle\Phi_m|\hat{J}_b|\Phi_n\rangle}{w+(E_n-E_m)/\hbar+\mathrm{i}\delta} \ \text{ with } \ \delta\to 0^+. \tag{23}$$

From the above expression we see that current response function solely depends on the CM eigenstates and the CM eigenenergies. This is a consequence of homogeneity which implies the separability of the full Hamiltonian into CM

and relative parts. Finally, for completeness we provide the expressions for the components of the current operator in terms of the polaritonic annihilation and creation operators

$$\begin{aligned}\hat{J}_x &= \frac{e^2\sqrt{N}B}{m_e^{3/2}}\sqrt{\frac{\hbar}{2(1+\Lambda^2)}}\left[\frac{\sqrt{m_e}}{eB}\left(-\mathrm{i}\hbar\nabla_X-\hbar K_x\right)+\frac{\Lambda+\eta}{\sqrt{\Omega_-}}\left(\hat{b}_-^\dagger+\hat{b}_-\right)+\frac{1-\eta\Lambda}{\sqrt{\Omega_+}}\left(\hat{b}_+^\dagger+\hat{b}_+\right)\right]\\ \hat{J}_y &= -\mathrm{i}e\sqrt{\frac{\hbar N}{2m_e(1+\Lambda^2)}}\left[\sqrt{\Omega_+}\left(\hat{b}_+-\hat{b}_+^\dagger\right)+\Lambda\sqrt{\Omega_-}\left(\hat{b}_--\hat{b}_-^\dagger\right)\right].\end{aligned} \tag{24}$$

With the above expressions one can use straightforwardly apply the Kubo formalism and compute the temperature dependent current response functions in Eq. 23 and the corresponding conductivities defined in Eq. 12. For more details on the finite temperature Kubo formalism for the Landau polariton states one can see Ref. [9].

VI. NO MODIFICATION OF QUANTUM HALL TRANSPORT AT $T = 0$

Having derived the general formula for the current correlator $\chi_{ab}(w)$ at finite temperature, we will focus now at the transport properties at zero temperature, $T = 0$, where the topological protection and the quantization of the quantum Hall conductance are expected from the Thouless argument, as long as the system is gapped [13]. At $T = 0$ the ground state of the polariton system is for $n_+ = n_- = 0$ and only the thermal prefactors corresponding to the ground state $e^{-\beta E_{00}}$ contribute to transport.

$$\chi_{ab}(w) = \sum_{m_+,m_-}\frac{\langle 00|\hat{J}_a|m_+m_-\rangle\langle m_+m_-|\hat{J}_b|00\rangle}{w+(E_{00}-E_{m_+m_-})/\hbar+\mathrm{i}\delta}-(00\leftrightarrow m_+m_-) \tag{25}$$

Furthermore, the current operators are linear in the polaritonic annihilation and creation operators and thus allow only for single-polariton transitions to occur, which implies that in the denominator of the response function only the single polariton energies $\Omega_\pm$ show up. Finally, using the formulas for the matrix representation of the components of the current operator we find the following analytically exact expressions for the transverse χ_{xy} response function

$$\chi_{xy}(w) = \frac{Ne^3B}{(1+\Lambda^2)m_e^2}\Big[\Lambda(\Lambda+\eta)\frac{\mathrm{i}}{2}\left(\frac{1}{w+\Omega_-+\mathrm{i}\delta}+\frac{1}{w-\Omega_-+\mathrm{i}\delta}\right)+(1-\eta\Lambda)\frac{\mathrm{i}}{2}\left(\frac{1}{w+\Omega_++\mathrm{i}\delta}+\frac{1}{w-\Omega_++\mathrm{i}\delta}\right)\Big] \tag{26}$$

With the above result and using the Kubo formula in Eq. 12 we find the Hall conductance by taking the limit $w \to 0$

$$\sigma_{xy} = \frac{e^2\nu}{h(1+\Lambda^2)}\left[\frac{\Lambda(\Lambda+\eta)}{\Omega_-^2/\omega_{\mathrm{cyc}}^2+\delta^2/\omega_{\mathrm{cyc}}^2}+\frac{1-\eta\Lambda}{\Omega_+^2/\omega_{\mathrm{cyc}}^2+\delta^2/\omega_{\mathrm{cyc}}^2}\right] \quad \text{where} \quad \eta=\omega_d/\omega_{\mathrm{cyc}}. \tag{27}$$

Where we introduced the Landau level filling factor $\nu = n_s h/eB$, as defined in the main text. Taking the value of the broadening parameter to zero $\delta \to 0$ we find that the Hall conductance is quantized

$$\sigma_{xy} = \frac{e^2\nu}{h}, \tag{28}$$

consistently with the Thouless flux insertion argument [13]. In the last step we used two properties of the mixing parameter $1-\eta\Lambda = \Omega_+^2/\omega_{\mathrm{cyc}}^2$ and $\Lambda(\Omega_-^2/\omega_{\mathrm{cyc}}^2-1)=\eta$ which can be exactly deduced from the definition of Λ.

A. Singular Point

We also comment on the limit where the cavity frequency ω_{cav} is much smaller than the other energy scales in the light-matter system, namely the diamagnetic frequency ω_d, and the cyclotron frequency ω_{cyc}, i.e. $\omega_{\mathrm{cav}} \ll \omega_d, \omega_{\mathrm{cyc}}$. In this limit, where the cavity frequency becomes negligible, it can be easily seen that the lower polariton mode goes to zero, $\Omega_- \to 0$, as it was found in Ref. [14]. Having the lower polariton gap closing circumvents the Thouless flux insertion argument [13] which assumes the system to be gapped. The gap closing leads to the modification of the Hall conductance as it was found in Ref. [15]. Finally, we note that in order to obtain the result in Eq. 28 the lower

polariton mode Ω_- needs to be non-zero at all steps of the calculation for the Hopfield transformation to the polariton basis to be well-defined. This can be understood by taking $\Omega_- \to 0$ in Eq. 27.

---

[1] F. Delahaye, Journal of Applied Physics **73**, 7914 (1993).
[2] F. Appugliese, J. Enkner, G. Paravicini-Bagliani, M. Beck, C. Reichl, W. Wegscheider, G. Scalari, C. Ciuti, and J. Faist, Science **375**, 1030 (2022).
[3] M. Fogler and B. Shklovskii, Solid state communications **94**, 503 (1995).
[4] J. Matthews and M. Cage, Journal of Research of the National Institute of Standards and Technology **110**, 497 (2005).
[5] V. Rokaj, D. M. Welakuh, M. Ruggenthaler, and A. Rubio, Journal of Physics B: Atomic, Molecular and Optical Physics **51**, 034005 (2018).
[6] C. Cohen-Tannoudji, J. Dupont-Roc, and G. Grynberg, *Photons and Atoms: Introduction to Quantum Electrodynamics* (Wiley, 1989).
[7] W. Kohn, Phys. Rev. **123**, 1242 (1961).
[8] J. J. Hopfield, Phys. Rev. **112**, 1555 (1958).
[9] V. Rokaj, J. Wang, J. Sous, M. Penz, M. Ruggenthaler, and A. Rubio, Phys. Rev. Lett. **131**, 196602 (2023).
[10] R. Kubo, J. Phys. Soc. Jpn. 12 (1957).
[11] P. Allen, in *Conceptual Foundations of Materials*, Contemporary Concepts of Condensed Matter Science, Vol. 2, edited by S. G. Louie and M. L. Cohen (Elsevier, 2006) pp. 165–218.
[12] L. D. Landau and E. M. Lifshitz, *Quantum Mechanics, Third Edition: Non-relativistic Theory* (Pergamon Press, 1997).
[13] D. J. Thouless, M. Kohmoto, M. P. Nightingale, and M. den Nijs, Phys. Rev. Lett. **49**, 405 (1982).
[14] V. Rokaj, M. Penz, M. A. Sentef, M. Ruggenthaler, and A. Rubio, Phys. Rev. Lett. **123**, 047202 (2019).
[15] V. Rokaj, M. Penz, M. A. Sentef, M. Ruggenthaler, and A. Rubio, Physical Review B **105**, 205424 (2022).